J. Fluid Mech. (2016), *vol.* 800, *pp.* 307–326.
doi:10.1017/jfm.2016.399

Existence of a sharp transition in the peak propulsive efficiency of a low-*Re* pitching foil

Anil Das[1], Ratnesh K. Shukla[1,†] and Raghuraman N. Govardhan[1,†]

[1]Department of Mechanical Engineering, Indian Institute of Science, Bangalore, 560012, India

(Received 12 November 2015; revised 16 April 2016; accepted 8 June 2016;
first published online 7 July 2016)

We perform a comprehensive characterization of the propulsive performance of a thrust generating pitching foil over a wide range of Reynolds ($10 \leqslant Re \leqslant 2000$) and Strouhal ($St$) numbers using a high-resolution viscous vortex particle method. For a given Re, we show that the mean thrust coefficient $\overline{C_T}$ increases monotonically with St, exhibiting a sharp rise as the location of the inception of the wake asymmetry shifts towards the trailing edge. As a result, the propulsive efficiency too rises steeply before attaining a maximum and eventually declining at an asymptotic rate that is consistent with the inertial scalings of St^2 for $\overline{C_T}$ and St^3 for the mean power coefficient, with the latter scaling holding, quite remarkably, over the entire range of Re. We find the existence of a sharp increase in the peak propulsive efficiency η_{max} (at a given Re) in the Re range of 50 to approximately 1000, with η_{max} increasing rapidly from about 1.7 % to the saturated asymptotic value of approximately 16 %. The St at which η_{max} is attained decreases progressively with Re towards an asymptotic limit of 0.45 and always exceeds the one for transition from a reverse von Kármán to a deflected wake. Moreover, the drag-to-thrust transition occurs at a Strouhal number St_{tr} that exceeds the one for von Kármán to reverse von Kármán transition. The St_{tr} and the corresponding power coefficient $\overline{C_{p,tr}}$ are found to be remarkably consistent with the simple scaling relationships $St_{tr} \sim Re^{-0.37}$ and $\overline{C_{p,tr}} \sim Re^{-1.12}$ that are derived from a balance of the thrust generated from the pitching motion and the drag force arising out of viscous resistance to the foil motion. The fact that the peak propulsive efficiency degrades appreciably only below $Re \approx 10^3$ establishes a sharp lower threshold for energetically efficient thrust generation from a pitching foil. Our findings should be generalizable to other thrust-producing flapping foil configurations and should aid in establishing the link between wake patterns and energetic cost of thrust production in similar systems.

Key words: propulsion, vortex shedding, wakes/jets

1. Introduction

Unsteady flapping foil based thrusters have emerged as ideal candidates for enabling propulsion in bio-inspired and bio-mimetic devices such as autonomous underwater

† Email addresses for correspondence: ratnesh@mecheng.iisc.ernet.in, raghu@mecheng.iisc.ernet.in

vehicles (Triantafyllou, Triantafyllou & Yue 2000). To a large extent, this emergence has been driven by the extensive utilization of undulatory body motions in a wide spectrum of small to medium-sized swimming aquatic organisms. The prevalence of unsteady flapping-like undulatory thrust generating motions is indicative of their efficacy over a vast range of Reynolds numbers (Re). Nevertheless, despite their versatility, unsteady flapping based thrust generation techniques remain vastly distinct from propulsive methods utilized by micro-sized organisms to overcome viscous drag at low Re (Lighthill 1975). This disparity between propulsive techniques used by tiny ($Re \ll 1$) and large ($Re \gg 1$) living organisms, suggests that a deterioration in propulsive efficiency is expected below a certain threshold Re for flapping foils that employ time-reversible kinematics to generate thrust. This argument is supported by the findings of Birch, Dickson & Dickinson (2004) who show that a reduction in Re from 1400 to 120 alters the flow topology significantly (also see Harbig, Sheridan & Thompson 2013), leading to an appreciable reduction in the hydrodynamic forces in a flapping wing configuration. Given the recent thrust towards miniaturization of autonomous underwater and micro-air vehicles, a quantification of the propulsive performance at low Re, and an inquiry into the existence of a threshold Re for performance deterioration in flapping foil based thrust generating systems is of utmost importance and is a prerequisite for their successful utilization in small scale self-propelling devices.

In this work, we investigate the existence of such a threshold of propulsive performance for a representative unsteady thrust generating configuration that consists of a single rigid pitching foil. In particular, we focus on establishing the dependency of the mean thrust, power consumption and propulsive efficiency on the prescribed kinematics (pitching frequency) at low and moderate Reynolds numbers ($10 \leqslant Re \leqslant 2000$). To begin with, we consider a fixed small angular amplitude of 5° that prevents flow separation at the leading edge, and a sinusoidal pitching profile for which the kinematics can be described simply through one single parameter, namely, the pitching frequency. Working in the aforementioned range of Re, we span a wide range of Strouhal numbers St (non-dimensional pitching frequency), for a clear identification of the efficiency peaks at each Re (§ 3). The peak efficiency trends allows us to conclusively establish the range of Re ($Re \gtrapprox 1000$) over which pitching foils produce thrust at low energetic cost. We observe a pronounced steep decline in peak efficiency from the global maximum asymptotic limit only below a threshold Re of 1000. In the process, we also uncover a link between the relatively steep intermittent rise in the propulsive efficiency and the transitions in the wake patterns. Subsequently, we examine the generality of our principal conclusions concerning efficiency of thrust generation by investigating the effect of pitching angle on the propulsive performance for four additional angular amplitudes of $\theta_0 = 2°$, 8°, 12° and 16° (§ 5).

Owing to their simplicity, pitching foils have been the subject of several experimental and simulation based investigations. Experimental and numerical investigations aimed at establishing the effect of pitching frequency on the wake and mean thrust characteristics of a NACA 0012 foil pitching about quarter chord with angular amplitudes of 2° and 4° at Re of 12 000 were undertaken in Koochesfahani (1989) and Ramamurti & Sandberg (2001), respectively. Improved estimates of the thrust produced by pitching foils at Re of 12 600 were obtained in Bohl & Koochesfahani (2009) from a momentum deficit analysis that takes into account the streamwise velocity fluctuations. In a recent experimental investigation Mackowski & Williamson (2015) report a peak propulsive efficiency of 12 % from load cell based direct

measurements of the forces and moment acting on a NACA 0012 foil undergoing pure pitching motion at $Re = 16\,600$.

Our interest, in contrast to these prior works, is in establishing an upper threshold of Re below which the propulsive efficiency deteriorates appreciably. Note that such a deterioration must necessarily occur since the isotropic action of viscous forces precludes the possibility of thrust generation from symmetric pitching motions in the viscosity dominated Stokes regime at $Re \ll 1$ (Scallop theorem). To our knowledge, an investigation aimed at establishing this practically relevant threshold of performance through a quantification of the energetic cost of thrust production from low Re pitching foils has not been undertaken until now. It is worth noting that the focus of prior low-Re pitching foil investigations by Godoy-Diana, Aider & Wesfreid (2008) and Schnipper, Andersen & Bohr (2009) (also see Godoy-Diana *et al.* 2009) was purely on wake transitions at fixed Re of approximately 10^3. As shown in § 4 of this paper, the specific case investigated in Godoy-Diana *et al.* (2008) appears as a trend line on a general two-dimensional regime map that we have presented in figure 8 to illustrate the significant impact of a variation in Re and St on the wake behind a sinusoidally pitching foil.

Pitching foils belong to the more general class of flapping foil based propulsive configurations that rely on combined pitch and heave motions to generate mean thrust. Thrust generating rigid and flexible foils undergoing pure heave and combined pitch and heave motions have received enormous attention (Katz & Weihs 1978; Anderson *et al.* 1998; Wang 2000; Lewin & Haj-Hariri 2003; Heathcote & Gursul 2007; Eldredge, Toomey & Medina 2010; Dewey *et al.* 2013; Zhu, He & Zhang 2014*a*,*b*; Quinn, Lauder & Smits 2015) due primarily to a strong connection with bio-locomotion (also see reviews of Triantafyllou *et al.* 2000; Shyy *et al.* 2010). In the present work, we study one of the more simple of these configurations, the pitching rigid foil, focussing our attention on the effect of Re at relatively small angular amplitudes ($\theta_0 \leqslant 16^\circ$). For this choice of θ_0, the leading edge of a purely pitching foil experiences only small displacements, limiting both the maximum effective angle of attack and flow separation at the leading edge. Consequently, complex interactions between the vortices shed from the leading and trailing edges are minimal so that the wake patterns and the intensities of the shed vortices are determined predominantly by the trailing edge excursions. The effective isolation of the leading and trailing edge effects in a small-amplitude pitching foil enables a more focused exploration of the connection between the energetic cost of thrust generation and the wake patterns. Nevertheless, we do expect that some of the broad results from the present work, especially the ones concerning the effect of Re on maximum propulsive efficiency, would extend to the other related configurations.

2. Problem definition and simulation methodology

The set-up we consider is similar to the one investigated by Koochesfahani (1989). We simulate the uniform incompressible flow of a Newtonian fluid with constant viscosity past a two-dimensional NACA 0012 foil undergoing sinusoidal pitching motion about its quarter chord. The set-up is described completely by the non-dimensional parameters $Re = U_\infty c/\nu$ and $St = fA/U_\infty$, where U_∞, c, ν, f and A denote free stream velocity, foil chord, kinematic viscosity of the fluid, pitching frequency and the peak-to-peak trailing edge displacement, which serves as a good indicator of the wake width (Triantafyllou *et al.* 2000). The instantaneous pitching angle $\theta = \theta_0 \cos(2\pi ft)$ with $\theta_0 = 5^\circ$. The influence of the amplitude of pitching angle θ_0 on thrust generation and flow characteristics is considered later in § 5.

Next, we introduce performance metrics to quantify the energetic cost of thrust production from the pitching foil. The non-dimensional thrust coefficient $C_T = 2T/(\rho U_\infty^2 c)$, where T and ρ represent the thrust force experienced by the foil and the density of fluid, respectively. Net power consumed in producing the thrust T is given by the non-dimensional power coefficient $C_P = -2M_z\dot{\theta}/(\rho U_\infty^3 c)$, where M_z is the instantaneous moment that acts on the foil about the pitching point at quarter chord and $\dot{\theta} = \mathrm{d}\theta/\mathrm{d}t$ denotes the angular velocity of the foil. The propulsive efficiency $\eta = \overline{C_T}/\overline{C_P}$ gives a quantitative measure of the energetic cost of thrust production, where an overbar has been used to indicate mean quantities obtained through averaging over sufficiently long time intervals.

To establish the dependence of $\overline{C_T}$, $\overline{C_P}$ and η on Re and St, we simulate the set-up described above with prescribed foil kinematics on an unbounded two-dimensional domain using a high-resolution viscous vortex particle method. Given the good agreement between experimental findings and predictions from two-dimensional numerical simulations at a substantially high Re of 12 000 (Ramamurti & Sandberg 2001; Mackowski & Williamson 2015), it is reasonable to expect that three-dimensional effects would remain insignificant over the Re and St range investigated here. We therefore expect our two-dimensional simulations to provide a fairly accurate description of the flow field associated with a pitching foil of infinite span.

The viscous vortex particle method (VVPM) (Cottet & Koumoutsakos 2000; Koumoutsakos 2005) employed in our simulations is very similar to that of Eldredge (2007). It approximates the time-dependent incompressible Navier–Stokes equations in their Lagrangian form employing a representation of the vorticity field with a distribution of discrete overlapping vortex particles that possess a finite core. The method allows for the creation and evolution of these particles in such a way that the vorticity generation at the foil surface and its diffusion and advection throughout the fluid domain are modelled accurately. The distinguishing features of the VVPM include its natural adaptivity, which is a direct consequence of the Lagrangian treatment, and the transparency in application over unbounded domains which eliminates the complications that could arise from the prescription of outflow boundary conditions. Except for some key advances in the implementation related aspects (such as integration with the GPU (graphics processing unit) accelerated fast adaptive multipole method of Goude & Engblom (2013)), which enables GPU-accelerated simulations employing multi-million particles to be run at an order of magnitude lower computational expense (compared to conventional CPU implementation), the methodology adopted in our work is the same as Eldredge (2007). Details of our GPU implementation along with results from comparative tests aimed at assessing the efficacy of the GPU implementation are provided in the accompanying supplementary material available at http://dx.doi.org/10.1017/jfm.2016.399.

3. Propulsive efficiency of thrust generation

We conduct simulations spanning the parametric space defined by $10 \leqslant Re \leqslant 2000$ and a wide range of St. Figure 1 depicts the mean thrust ($\overline{C_T}$) and power coefficients ($\overline{C_P}$) as a function of St obtained from these simulations over a range of Re. At zero St, the foil remains stationary and experiences a net drag force represented by a corresponding drag coefficient (C_{D0}), which decreases with Re as seen in figure 1(*a*). We find the variation of C_{D0} with Re to be of the form $C_{D0} = 5.91Re^{-0.56}$, where the exponent -0.56 is found to be close to the $1/\sqrt{Re}$ form, indicative of the dominance of viscous forces from the unseparated boundary layer over the stationary streamlined

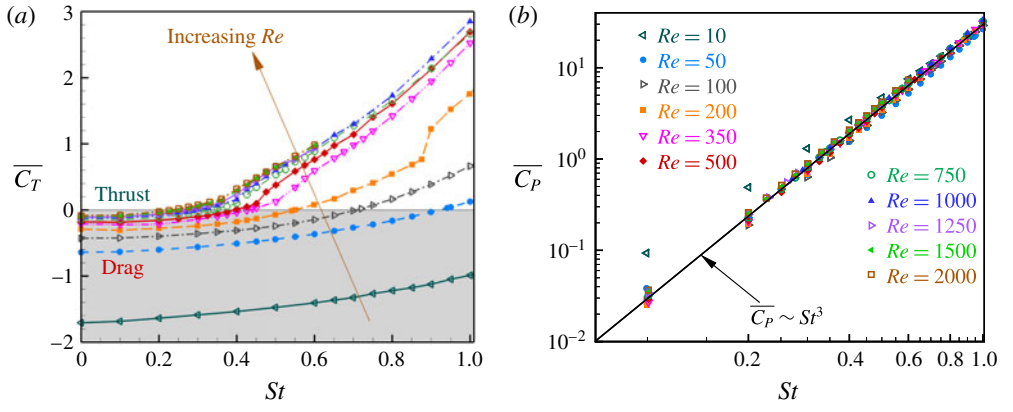

FIGURE 1. (Colour online) Time-averaged (*a*) thrust and (*b*) power coefficients as a function of St for varying Re at a fixed $\theta_0 = 5°$. Solid line in (*b*) is a cubic fit through the discrete data points.

foil surface. An increase in St results in a gradual decrease in the total drag. For a given Re, beyond a threshold St, a crossover from drag to thrust ($\overline{C_T} > 0$) is observed. We denote the critical St for drag-to-thrust transition by $St_{tr} = St(C_T = 0)$. At a given St, the mean thrust produced from the pitching motion rises substantially with an increase in Re over the range $Re \leqslant 350$. Subsequently, at $Re > 350$, the rise in $\overline{C_T}$ with further increments in Re becomes increasingly insignificant, which suggests a transition from viscous-to-inertial scaling for $\overline{C_T}$ at sufficiently high St and Re. In contrast, the power consumed in sustaining the pitching motions ($\overline{C_P}$) exhibits a strong inertial scaling of St^3 (also see the explanation below) that is almost insensitive to a change in Re (figure 1*b*).

Figure 2(*a*) illustrates the propulsive efficiency η computed from the ratio of $\overline{C_T}$ and $\overline{C_P}$ depicted in figure 1. At low St, the propulsive efficiency remains negative as the foil experiences a net drag. For $St > St_{tr}$, η becomes positive and continues to rise further with St. At each Re, a distinct sharp increment in efficiency is clearly evidenced from figure 2(*a*). The specific St at which this sharp increase in η occurs decreases with Re and is intricately linked to the extent of wake deflection (see § 4). For more rigorous pitching at moderate St, the rate of increase of $\overline{C_P}$ overwhelms that of $\overline{C_T}$ so that the efficiency decreases after attaining a maximum. We denote this maximum η and the corresponding Strouhal number by η_{max} and St_{max}, respectively. For sufficiently large St, the high intensity of pitching yields inertial scalings of the form $\overline{C_T} \sim St^2$ and $\overline{C_P} \sim St^3$, which are reflected in the asymptotic behaviour of η at large St ($\eta \sim St^{-1}$ for $Re \geqslant 1000$ and $St > 0.6$ as shown in figure 2*a*). The aforementioned scaling laws for $\overline{C_T}$, $\overline{C_P}$ and η at high St can be derived from physical arguments as shown later in this section. It may be noted here that this trend persists even at lower $Re = 10$, 50 and 100, but occurs at higher St that extends beyond the range ($St \leqslant 1$) illustrated in figure 2(*a*). The general form of dependency of η on St observed in our work is consistent with earlier experimental investigations on pitching foils (Dewey *et al.* 2013; Mackowski & Williamson 2015), and other flapping foil motions (Anderson *et al.* 1998; Lewin & Haj-Hariri 2003; Heathcote & Gursul 2007).

The crossover from negative to positive propulsive efficiencies allows for a clear identification of St_{tr} for drag-to-thrust transition from figure 2(*a*). It is possible to derive a relationship that expresses the dependency of drag-to-thrust transition Strouhal

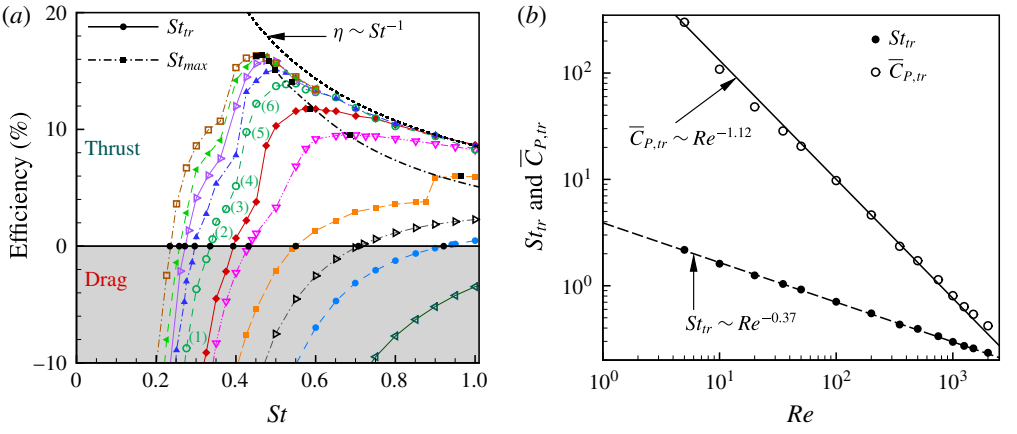

FIGURE 2. (Colour online) (*a*) Propulsive efficiency η as a function of St for varying Re at a fixed $\theta_0 = 5°$. The symbols and lines that are used to distinguish between different Re are the same as in figure 1. For each Re, the points corresponding to drag-to-thrust transition and maximum η are marked with (●) and (■), respectively. The dotted black line represents a large St upper envelope of all the η versus St curves associated with constant Re. The dash dots (–·–·–) indicate a fit through the points (■) associated with maximum η. (*b*) Drag-to-thrust transition Strouhal number St_{tr} (●) and corresponding mean power coefficient $\overline{C_{P,tr}}$ (○) as a function of Re.

number St_{tr} on Re by considering a balance between the time-averaged drag force arising out of skin friction that acts along the foil surface, and the thrust generated from the time-periodic sinusoidal pitching motion. To arrive at such a relationship we first derive expressions that relate time-averaged drag force and the thrust generated to the kinematic parameters and fluid properties as shown below.

An estimate for the viscous resistance to the foil motion must account for a potential increase in the skin friction due to a reduction in the boundary layer thickness on the surface towards which the rigid airfoil moves. Application of the Bone–Lighthill boundary layer thinning hypothesis (Lighthill 1971; Ehrenstein & Eloy 2013; Ehrenstein, Marquillie & Eloy 2014) then leads to the following estimate

$$\overline{D_A} \sim \rho U_\infty^2 c Re^{-0.56} \sqrt{\overline{|U_N^*|}}, \quad \overline{|U_N^*|} = \overline{|U_N|}/U_\infty \tag{3.1a,b}$$

for the cycle-averaged axial (longitudinal) drag force per unit length $\overline{D_A}$ experienced by the foil, where $\overline{|U_N|}$ represents the mean absolute value of the normal foil velocity (Ehrenstein *et al.* 2014) and the exponent of Re is in accord with the previously obtained scaling exponent for C_{D0}. Furthermore, since $\overline{|U_N|} \sim Af$ we obtain the mean axial drag coefficient

$$\overline{C_D^{(A)}} = \frac{2\overline{D_A}}{\rho U_\infty^2 c} \sim Re^{-0.56}\sqrt{St}. \tag{3.2}$$

To obtain an expression for the thrust generated by the foil motion we follow the arguments outlined in Gazzola, Argentina & Mahadevan (2014). The pitching motion of the airfoil induces a local fluid acceleration that scales as Af^2. The resulting reaction force exerted on the airfoil by the surrounding fluid therefore scales as

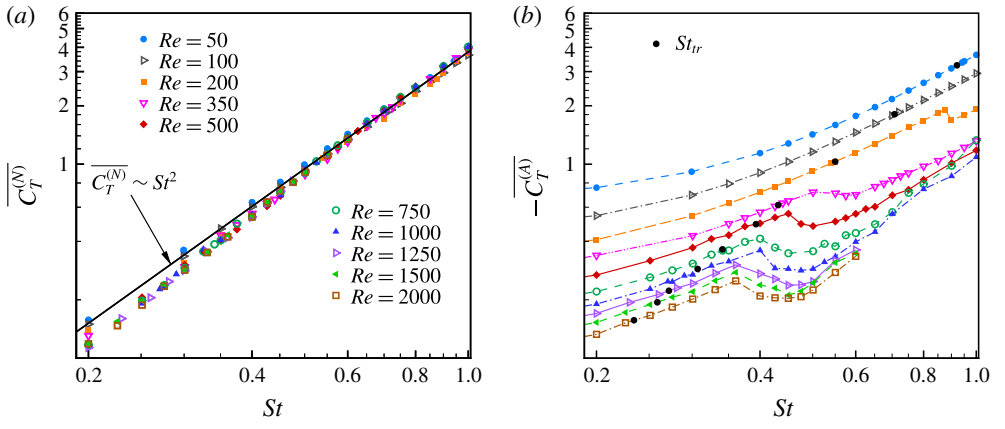

FIGURE 3. (Colour online) The mean (*a*) normal and (*b*) axial thrust coefficients ($\overline{C_T^{(N)}}$ and $\overline{C_T^{(A)}}$, respectively) as a function of St for varying Re at a fixed $\theta_0 = 5°$.

$\rho c^2 A f^2$. Furthermore, since the angle between the foil axis and the free stream $\sim A/c$, the thrust generated from the pitching action of the airfoil is given by $\overline{T_N} \sim \rho c A^2 f^2$. The mean normal thrust coefficient therefore assumes the following form:

$$\overline{C_T^{(N)}} = \frac{2\overline{T_N}}{\rho U_\infty^2 c} \sim St^2. \tag{3.3}$$

At drag-to-thrust transition, a balance between the mean normal thrust coefficient and the cycle-averaged axial drag coefficient ($\overline{C_T^{(N)}} = \overline{C_D^{(A)}}$) yields $St_{tr} \sim Re^{-0.37}$. We find that the discrete data points for St_{tr} at various Re obtained from our simulation runs are in remarkable consistency with the scaling law derived above (see figure 2*b*). Moreover, for this self-propelling state, we find that the mean power coefficient $\overline{C_{P,tr}} = \overline{C_P}(\overline{C_T} = 0)$ too can be expressed through a simple relationship: $\overline{C_{P,tr}} \sim Re^{-1.12}$, the Re exponent in this case being 3 times the Re exponent for St_{tr}. This again is in accordance with our earlier observation and the analysis presented below in that $\overline{C_P} \sim St^3$.

To further assess the validity of the scaling laws derived above, we illustrate the dependence of the mean axial ($\overline{C_T^{(A)}}$) and normal ($\overline{C_T^{(N)}}$) contributions to the net thrust, on St, for varying Re in figure 3. The fact that the normal contribution $\overline{C_T^{(N)}}$ is thrust producing and, more importantly, scales as St^2 independently of Re, lends support to the expression (3.3) derived from physical arguments. Furthermore, we find that the axial contribution $\overline{C_T^{(A)}}$ to be negative and drag producing in accordance with the prior findings and the Bone–Lighthill boundary layer thinning hypothesis (Lighthill 1971; Ehrenstein & Eloy 2013; Ehrenstein *et al.* 2014). Moreover, the drag-producing axial contribution $-\overline{C_T^{(A)}}$ exhibits a strong Re dependence and monotonic increase with St before, up to and slightly beyond the drag-to-thrust transition point just before the onset of significant asymmetry in the wake. This is again consistent with the expected Re-dependent increase in the viscous resistance to the airfoil motion owing to a reduction in the boundary layer thickness on the surface towards which the rigid airfoil moves during the half-cycle (Lighthill 1971; Ehrenstein & Eloy 2013;

Ehrenstein *et al.* 2014). It is worth noting that the estimate for $\overline{C_D^{(A)}}$ (or equivalently $\overline{C_T^{(A)}} = -\overline{C_D^{(A)}}$) given by (3.2) has a limited range of applicability. In particular, the estimate is certainly not applicable in the limit $St \to 0$, in which case the boundary layer thickness is determined by the free stream velocity and not the vanishingly small normal foil velocity. Moreover, beyond a certain St, the wake deflection becomes significant so that the pressure contribution to the axial thrust becomes increasingly important. The expression (3.2) which considers contributions from skin friction drag only is certainly not applicable in such scenarios.

Interestingly, the scaling law of $St_{tr} \sim Re^{-0.37}$ derived for drag-to-thrust transition in the present rigid pitching airfoil configuration differs markedly from the scaling law of $St \sim Re^{-0.25}$ for undulatory propulsion that is obtained from a balance of normal thrust and viscous resistance without accounting for the normal motion-induced reduction in the boundary layer thickness (Gazzola *et al.* 2014). The difference between these two scaling laws is indicative of the disparity between the present set-up that relies on pure rigid pitching motions and aquatic locomotion where a reduction in boundary layer thickness is most likely prevented through travelling-wave-like undulatory motion of flexible tails. Nonetheless, our simulation results and the analysis above clearly indicate that a St-dependent normal surface-motion-induced reduction in the boundary layer thickness and a corresponding increase in the viscous resistance are both expected to prevail in configurations wherein rigid surfaces undergo motion perpendicular to the free stream direction.

At relatively high St, the mean normal contribution to the thrust is expected to completely overwhelm the drag-producing axial contribution. In such cases, since $\overline{C_T} \approx \overline{C_T^{(N)}}$, as evident from figure 3(*a*), one would expect the mean thrust generated from the pitching motion to follow the scaling law $\overline{C_T} \sim St^2$. Moreover, since the moment $M_z \sim St^2$, one obtains $\overline{C_P} \sim St^3$ in good accord with the trends depicted in figure 1(*b*). Thus, for sufficiently high St, the scaling laws for $\overline{C_T}$ and $\overline{C_P}$ yield $\eta \sim St^{-1}$ in good agreement with the propulsive efficiency trends depicted in figure 2(*a*).

The efficiency trends depicted in figure 2(*a*) also allow for an explicit identification of the maximum achievable efficiency η_{max} and the corresponding Strouhal number St_{max} for each Re, as shown in figure 4. In the viscosity dominated regime ($Re \ll 1$), the symmetric action of the pitching foil produces no thrust so that the corresponding η_{max} is expected to remain negligibly small. With increase in Re, η_{max} rises gradually from about 0.65 % at $Re = 10$ to almost 1.71 % at $Re = 50$. For intermediate $Re \sim O(10^2)$, η_{max} rises sharply reaching 15.1 % at $Re = 10^3$. In particular, a rapid rise in η_{max} is observed between $Re = 100$ and 350, with the enhancement in η_{max} diminishing substantially for $Re > 350$. Beyond $Re = 1000$, η_{max} remains largely unchanged and saturates to an upper threshold of approximately 16 % as shown in figure 4(*a*). The corresponding Strouhal number for peak propulsive efficiency also exhibits a similar trend, with St_{max} decreasing monotonically with Re, and reaching an asymptotic value of about 0.45 (see figure 4*b*).

The global maximum peak efficiency estimate of 16 % from our simulations is in fairly good agreement with the peak efficiencies of 16 % for a flat plate pitching about its leading edge at $Re = 7200$ (Dewey *et al.* 2013, experiments) and 18 % for a NACA 0012 foil pitching about its quarter chord at $Re = 13\,500$ (Lu *et al.* 2013, two-dimensional simulations). Our global maximum of 16 % is higher than the maximum efficiency of 12 % reported in the experiments of Mackowski & Williamson (2015) for a set-up similar to ours, but for an amplitude of 8° at higher $Re = 16\,600$. This discrepancy may be due to the smaller range of Strouhal numbers investigated in their

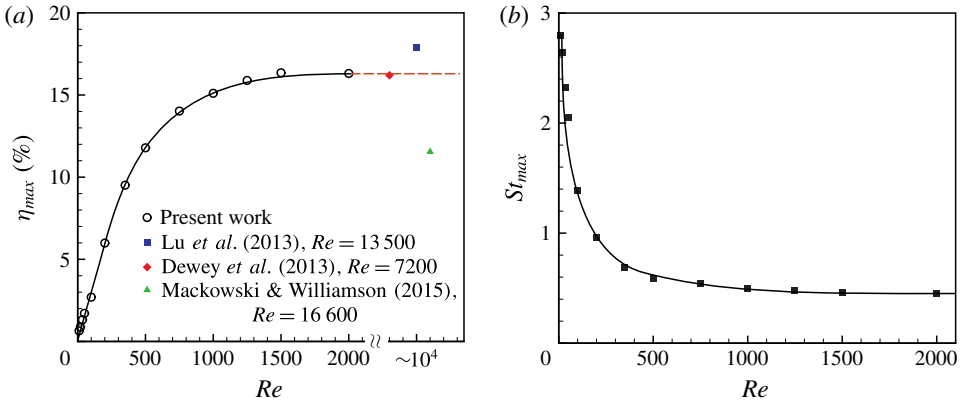

FIGURE 4. (Colour online) Variation with Re of (a) the maximum efficiency (η_{max}) and (b) the corresponding Strouhal number (St_{max}) at $\theta_0 = 5°$ for the present work and prior investigations on pitching foils at higher Re. Lu, Xie & Zhang (2013) and Mackowski & Williamson (2015) investigate a NACA 0012 foil pitching about its quarter chord with $\theta_0 = 5°$ and 8°, respectively. Dewey *et al.* (2013) examine a truncated foil with a flat plate pitching about its leading edge, attached to its rear.

experiments ($St < 0.33$), with our simulations predicting a St_{max} value of approximately 0.45 at high Re.

The asymptotic St_{max} of 0.45 obtained from our present investigation is on the higher side and lies outside the St range of 0.2–0.4 that generally holds for high propulsive efficiency undulatory bio-locomotion (Taylor, Nudds & Thomas 2003). The fact that the asymptotic limit of $St_{max} = 0.45$ determined in our work is higher than the upper limit of 0.4 for undulatory propulsion is consistent with the expectation that the optimal St for high-efficiency thrust generation would in general exceed the optimal St for energetically efficient self-propulsion. Moreover, over the moderate Reynolds numbers range of $500 \leqslant Re \leqslant 2000$, we observe that the drag-to-thrust transition Strouhal number St_{tr} corresponding to a self-propelling pitching foil decreases monotonically from 0.39 (at $Re = 500$) to 0.23 (at $Re = 2000$, see figure 2*b*). Thus, for $500 \leqslant Re \leqslant 2000$, St_{tr} lies well within the Strouhal number range of 0.2–0.4 for high-efficiency self-propulsion, in accordance with the observation of Taylor *et al.* (2003).

4. Wake characterization

Variations in Re and St induce systematic changes in the wake that are reflected in the sizes and arrangement of shed vortices. These changes in the wake signature are quite informative and provide useful insights into both thrust production and propulsive efficiency characteristics of the pitching foil. Figure 5(*a*) illustrates the sensitivity of the wake to variations in Re through the instantaneous vorticity contours at a fixed $St = 0.4$. At low $Re \leqslant 200$, the dominance of viscosity is clearly evidenced in the thick boundary layers that are formed at the foil surface and the localized trailing edge vortices which dissipate rapidly within a few chord lengths in the near wake. The harmonic motion of the trailing edge leads to formation of the classical von Kármán vortex street at $Re = 50$, 100 and 200 that is aligned with the free stream. With increase in Re, the wake undergoes a transition from von Kármán to reverse

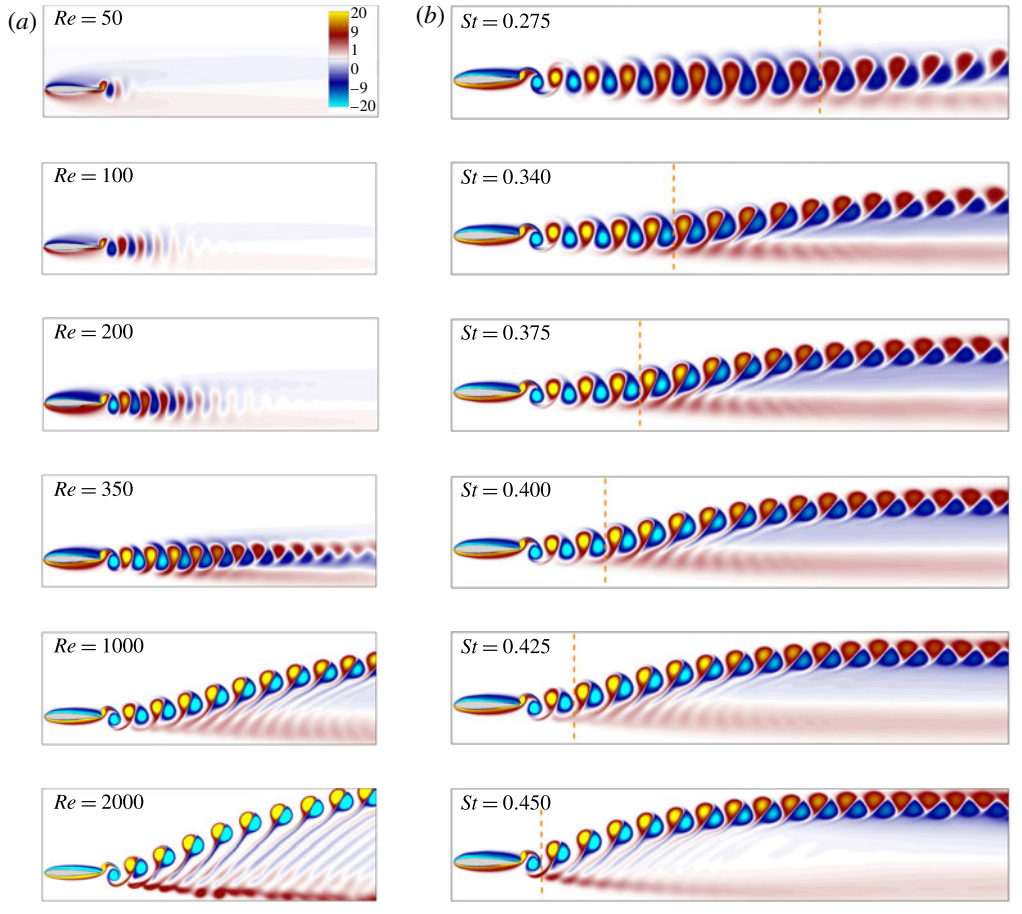

FIGURE 5. (Colour online) Effect of (*a*) Re at $St = 0.4$ and (*b*) St at $Re = 750$ on the vorticity field for a fixed $\theta_0 = 5°$. Dashed vertical lines (orange) indicate the location at which an appreciable asymmetry can be detected in the arrangement of the wake vortices. The six wake patterns in (*b*) at $Re = 750$ correspond to the points (1) to (6) marked in figure 2(*a*).

von Kármán vortex street as evidenced from a switch in the relative positions of the clockwise and counter-clockwise vortices with respect to the centreline at $Re = 350$ (see figure 5*a*). Our classification of wake vortices into the two distinct categories of classical and reverse von Kármán vortex street is based on not just the arrangement of vortices but also on the direction of the jet flow that is produced in the wake of the pitching foil, in a reference frame attached to the free stream. Throughout this work, we have labelled the wake vortices to be classical or reverse von Kármán depending on whether this jet is directed against (forward jet) or along (rear jet) the flow direction. With further increase in Re, the vortex street develops asymmetry and deflects upwards at an angle with respect to the free stream. The wake deflection is intensified and the strength of shed vortices progressively enhanced between $Re = 350$ and 2000.

The complex interplay between viscous and inertial effects that gives rise to the wake transitions is more clearly revealed in figure 5(*b*) through an illustration of

the effect of St on wake dynamics at a fixed $Re = 750$. The propulsive efficiency (η) corresponding to the 6 cases shown here may be seen from the corresponding points marked (1) to (6) in figure 2(*a*). At a low pitching frequency, corresponding to $St = 0.275$, the wake is already in the form of a reverse von Kármán street, but with a net drag (point (1) in figure 2*a*). With an increase in St, the thrust production rises monotonically, and we find the wake patterns to be discernibly more asymmetric downstream of the foil. Even at $St = 0.275$, one can see asymmetry developing approximately 4 chord lengths downstream of the foil (marked using the dashed vertical line (orange)). However, with increase in St, the location at which the asymmetry becomes appreciable (marked using the vertical dashed lines (orange)) shifts continuously towards the trailing edge. A careful inspection of the efficiency trends depicted in figure 2(*a*), and the wake patterns depicted in figure 5(*b*), indicates that pronounced increments that are observed in the efficiency around $St \approx 0.4$ correspond directly to the increased interaction between the pitching foil and the deflected wake owing to the shift in the location of asymmetry. For $St = 0.450$, the asymmetry sets in almost at the trailing edge of the pitching foil and further increments in St lead to only marginal gains in the efficiency of thrust production (see figure 2*a*).

In general, the net time-averaged force exerted on the airfoil can be resolved into components along and perpendicular to the direction of the free stream. In the deflected wake regime, the component perpendicular to the direction of the free stream does not vanish and results in a mean lift. Since only a fraction of the net force exerted on the airfoil is converted into a net thrust, one would expect $\overline{C_T}$ to actually decrease after the onset of wake deflection. In this sense, the steep increase in $\overline{C_T}$ and η with wake deflection and the occurrence of peak efficiency in the deflected wake regime are both counter-intuitive.

To shed light on the link between the observed enhancement in the mean thrust coefficient and the increased interaction between the airfoil and the deflected wake, we analyse the change in pressure and viscous contributions to the total thrust with rising St at a fixed Re of 750. As shown in figure 6(*a*), the viscous contribution to the net thrust ($\overline{C_T^{(v)}}$) is negative for a stationary airfoil ($St = 0$) and decreases further with an increase in St. Thus, the viscous stresses lead to a net drag that rises gradually with increasing St. The monotonic increase in $-\overline{C_T^{(v)}}$ with St is indicative of an overall decrease in the boundary layer thickness on the surface towards which the rigid airfoil moves during the half-cycle and is consistent with prior findings and the Bone–Lighthill boundary layer thinning hypothesis (Lighthill 1971; Ehrenstein & Eloy 2013; Ehrenstein *et al.* 2014).

In contrast, the pressure contribution to the net thrust ($\overline{C_T^{(p)}}$) is positive for almost all St (except for very small St for which the drag-producing pressure and viscous contributions combine to yield a negative thrust). The rate of increase of $\overline{C_T^{(p)}}$ with St overwhelms the rate at which $\overline{C_T^{(v)}}$ decreases and rises sharply beyond $St \approx 0.4$ (see figure 6*a*). Moreover, beyond $St \approx 0.4$, the location at which an appreciable asymmetry in the arrangement of shed vortices can be detected moves to within a cord length from the airfoil trailing edge. Thus, the increased interaction between the pitching airfoil and the deflected wake leads to a sharp rise in $\overline{C_T^{(p)}}$ and therefore $\overline{C_T}$. The reduction in proximity between the location of the wake deflection and the airfoil's trailing edge, however, has no noticeable influence on the drag-producing viscous contribution $\overline{C_T^{(v)}}$.

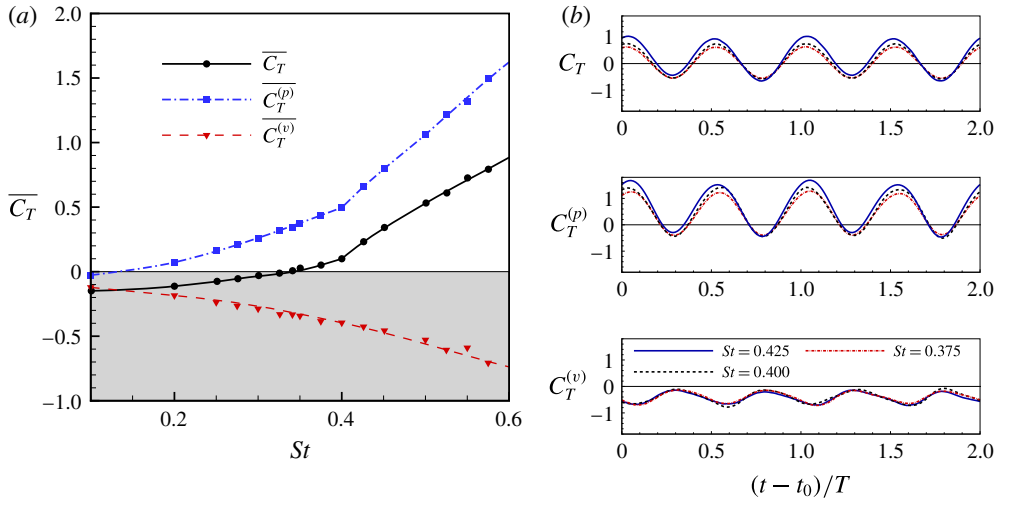

FIGURE 6. (Colour online) (*a*) Time-averaged thrust coefficient ($\overline{C_T}$) and the pressure and viscous contributions ($\overline{C_T^{(p)}}$ and $\overline{C_T^{(v)}}$, respectively) as a function of St at $Re = 750$ and $\theta_0 = 5°$. (*b*) Thrust coefficient (C_T) and the pressure and viscous contributions to the thrust coefficient ($C_T^{(p)}$ and $C_T^{(v)}$, respectively) as a function of time at $Re = 750$ and $\theta_0 = 5°$ for $St = 0.375$, 0.400 and 0.425. Here, T denotes the time period of pitching motion and $t_0 \gg T$.

The temporal variations of the instantaneous pressure and viscous contributions to $\overline{C_T}$ at $St = 0.375$, 0.4 and 0.425, as shown in figure 6(*b*), clearly indicate that the sharp increase in the mean $\overline{C_T^{(p)}}$ (and therefore $\overline{C_T}$) results from a prominent rise in the peak $C_T^{(p)}$. In particular, an increase in St from 0.375 to 0.400 leads to only a marginal rise in the peak $C_T^{(p)}$ and C_T. However, a further increase in St by the same amount from 0.400 to 0.425 results in a much more prominent increase in the peak $C_T^{(p)}$, the rise being maximum at time instants that correspond to phases of 180° and 0° for which the foil attains its extreme angular positions. On the contrary, the minimum $C_T^{(p)}$ exhibits no appreciable change with St. The viscous contribution to the net thrust $C_T^{(v)}$ too remains relatively insensitive to the changes in St from 0.375 to 0.4 and 0.425. In essence, the steep increase in the time-averaged thrust coefficient $\overline{C_T}$ for $St \gtrapprox 0.4$ is directly linked to a sharp rise in both the mean and the peak $C_T^{(p)}$.

The sharp rise in the $C_T^{(p)}$ between $St = 0.4$ and 0.425 is observed at time instants that correspond to the maximum airfoil acceleration. A close inspection of the flow field in the vicinity of the leading edge at the lowermost position of the airfoil's leading edge (0° phase) reveals a substantial change in the vorticity distribution between $St = 0.4$ and 0.425 cases (see figure 7*a*). Furthermore, the reduced proximity between the location corresponding to the onset of wake deflection and the airfoil's trailing edge leads to a stronger interaction between the boundary layer on the airfoil surface and the asymmetrically shed vortices. These deflected wake-induced changes in the vorticity distribution in the vicinity of the leading edge have a significant impact on the pressure contribution to the thrust coefficient.

To quantify the effect of variations in the vorticity distribution at the leading edge on cycle-averaged $C_T^{(p)}$, we define $C_{T,LE}^{(p)}$ as the leading edge contribution to $C_T^{(p)}$

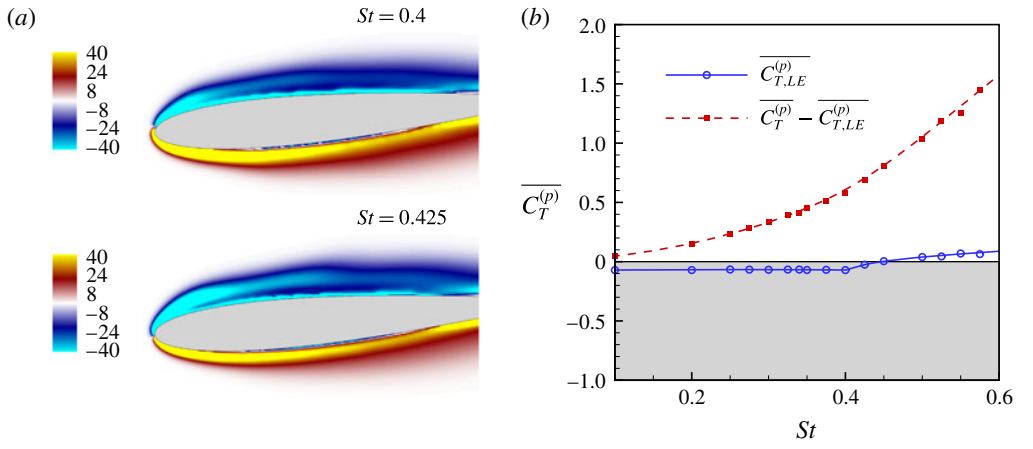

FIGURE 7. (Colour online) (*a*) Vorticity field in the vicinity of the leading edge of the airfoil for $St = 0.4$ and 0.425 at $Re = 750$, $\theta_0 = 5°$ and a phase of 0° (corresponding to the lowermost position of the airfoil's leading edge). (*b*) Contributions to $\overline{C_T^{(p)}}$ from the airfoil's leading edge ($\overline{C_{T,LE}^{(p)}}$) and the remaining section behind the pivot point ($\overline{C_T^{(p)}} - \overline{C_{T,LE}^{(p)}}$) as a function of St at $Re = 750$ and $\theta_0 = 5°$.

obtained by integrating the pressure distribution (vorticity flux in vortex methods, see Wu, Ma & Zhou (2007)) over the portion of the airfoil surface that lies ahead of the pivot point (between the pivot point and the leading edge). Figure 7(*b*) depicts $\overline{C_{T,LE}^{(p)}}$ and the time-averaged contribution to $\overline{C_T^{(p)}}$ from the airfoil section behind the pivot point ($\overline{C_T^{(p)}} - \overline{C_{T,LE}^{(p)}}$) as a function of St at a fixed Reynolds number of 750. We find that for $St \in (0.1, 0.4)$, the leading edge contribution $\overline{C_{T,LE}^{(p)}}$ amounts to a net drag that remains insensitive to the changes in the wake pattern (von-Kármán to reverse von Kármán). Beyond $St \gtrapprox 0.4$, however, the interaction of the pitching foil with the asymmetric wake leads to a sharp rise in $\overline{C_{T,LE}^{(p)}}$ and an eventual crossover from drag production to thrust generation ($\overline{C_{T,LE}^{(p)}}$ undergoes sign inversion). In contrast, the section behind the pivot point contributes to a net thrust that rises gradually with St for all $St > 0.1$.

The trends described above allow us to conclusively establish that the sharp increase in the pressure contribution to the thrust generated at the leading edge, owing to a strong interaction between the pitching foil and the deflected wake, is the principal reason behind the steep rise in cycle-averaged thrust coefficient. Clearly the steep rise in the pressure contribution more than compensates for not just the increase in viscous drag with St but also the inevitable loss in thrust that results from a fraction of excess wake momentum being converted to mean lift in the deflected wake regime. Moreover, as evidenced from figure 1(*b*), $\overline{C_P}$ increases only gradually with St over the entire range $0 \leqslant St \leqslant 1$, for all Re, and, unlike $\overline{C_T}$, exhibits no sharp variation with St. Hence, the relatively sharp increase in $\overline{C_T}$ with decreasing proximity between the mean position of the trailing edge and the location associated with the onset of significant wake deflection translates directly to a steep rise in the propulsive efficiency η (as observed from figure 2*a*).

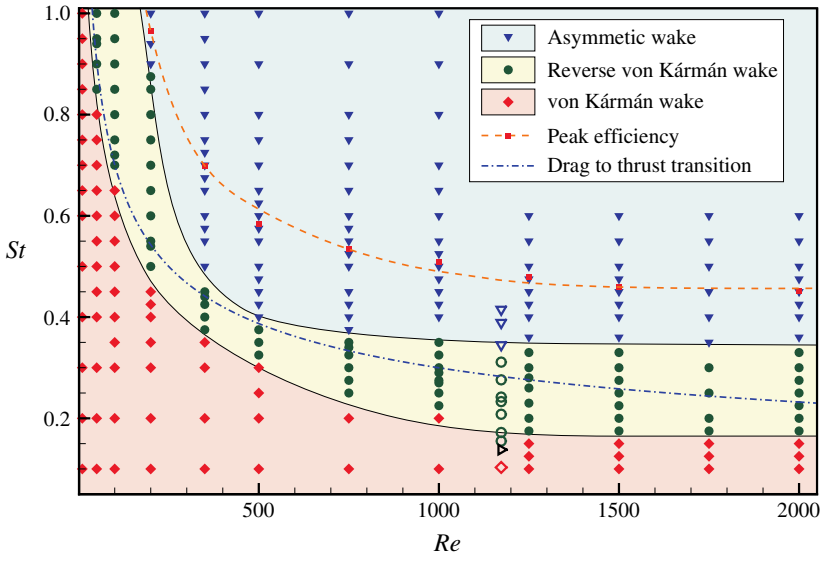

FIGURE 8. (Colour online) Wake map illustrating the three different wake patterns associated with a pitching foil as a function of St and Re for a fixed $\theta_0 = 5°$. Also shown are the drag-to-thrust transition St_{tr} line (blue) and the line on which the efficiency is maximum for a given Re (orange). Closed and open symbols indicate the results from the present work and those from Godoy-Diana *et al.* (2008), respectively. ▷ indicates aligned vortices in Godoy-Diana *et al.* (2008).

Figure 8 presents a comprehensive summary of the various wake patterns over the entire parametric space of St and Re in the form of a regime map. Depending on the parameters Re and St, the wake exhibits qualitatively different patterns that can be distinguished by the arrangement of the shed vortices and their inclination with respect to the free stream. For a given Re below a critical St ($St < 0.22$ at $Re = 750$, for instance), the classical von Kármán vortex street is formed in the wake of the pitching foil. Above this critical St, a transition from the regular von Kármán to a reverse von Kármán wake characterized by excess momentum is observed. As seen in figure 5(*b*), the reverse von Kármán wake exhibits asymmetry about the centreline at higher St. We classify wakes as asymmetric when an appreciable deflection in the arrangement of wake vortices can be detected at approximately 2.5 chord lengths. With this definition, we find that at $Re = 750$, wakes for $St \gtrapprox 0.37$ are asymmetric wakes. At very low Re such as $Re = 10$, a von Kármán vortex street forms for all $St < 1$; a transition to the reverse von Kármán vortex street does occur but only at significantly higher $St = 1.5$. As the Re is increased, the St at which a transition from a von Kármán to a reverse von Kármán and from a reverse von Kármán to a deflected wake takes place decreases sharply for $Re \lessapprox 10^3$. For $Re > 1000$, these transitions seem to occur at St of 0.17 and 0.35 that remains largely unchanged with further increments in Re. The invariance of wake transitions with respect to Re beyond $Re \gtrapprox 10^3$ is indicative of the ever growing dominance of inertial effects. This is also supported by the experimental observations of Ohmi *et al.* (1991) on a related pitching foil set-up but with high mean angles of attack, which show that the St for wake transitions is insensitive to Re in the range of 1500–10 000.

Figure 8 also illustrates the trends for drag-to-thrust transition ($St_{tr} = St_{tr}(Re)$) and peak efficiency ($St_{max} = St_{max}(Re)$). As seen in the figure, the transition from a

von Kármán to a reverse von Kármán wake does not occur along the drag-to-thrust transition curve as also pointed out by Godoy-Diana *et al.* (2008). Further, the peak propulsive efficiency is attained in the asymmetric wake region corresponding to a deflected vortex street. The wake transition predictions from the present investigation are broadly in agreement with the experimental study of Godoy-Diana *et al.* (2008) at $Re = 1150$ also shown in the figure, the minor differences being likely related to the differences in foil shape and pitching amplitude between the two studies.

5. Effect of pitching amplitude

The results so far presented in this study have all been at a fixed angular oscillation amplitude (θ_0) of 5°. A natural question that arises then is the effect of the angular oscillation amplitude (θ_0) on the results presented so far. At higher θ_0 values, one of the important changes expected from the flow side is the formation of a leading edge vortex, as has been discussed for example in McCroskey (1982) and Ohmi *et al.* (1991) for airfoils rapidly pitching at higher angles of attack. With the broad objective of examining the generality of our principal results concerning thrust generation, deduced from simulation runs at a fixed $\theta_0 = 5°$, we now investigate the effect of pitching angle on the propulsive performance for four additional angular amplitudes of $\theta_0 = 2°$, 8°, 12° and 16°.

The formation of a leading edge vortex at higher θ_0 values may be seen from the close up of the vorticity field around the airfoil depicted in figure 9(*a*). All the plots shown in this figure are at the same $St = 0.4$ and $Re = 750$ and correspond to the same phase of the airfoil motion, with the only difference being the variation of θ_0. For an unambiguous identification of the leading edge vortex formation, we have superposed on the vorticity fields in figure 9 the local peak in the Q-criterion (indicated using filled circles (•)). In the past, the Q-criterion (Hunt, Wray & Moin 1988) has been extensively employed for identification of vortical structures in a variety of complex flow fields. At relatively large angular amplitudes of 8°, 12° and 16°, the Q-criterion clearly identifies the centre of the leading edge vortex formed on the upper half of the airfoil, besides the one formed on the lower half. After formation near the leading edge, this vortex travels along the airfoil surface, unlike in the heaving case, where the leading edge vortex separates from the airfoil surface (Wang 2000; Lewin & Haj-Hariri 2003; Heathcote & Gursul 2007). In the present pitching case, this leading edge vortex first interacts with the boundary layer as it traverses along the airfoil surface and then eventually becomes a part of the vortex shed from the trailing edge, influencing the wake formation downstream, as noted by Ohmi *et al.* (1991) for a pitching foil at high angles of attack. The corresponding distribution of shed vortices in the wake region further downstream in each of the cases is illustrated in figure 9(*b*). As θ_0 is increased from 2°, the wake is seen to progressively become more symmetric, with the location at which the asymmetry is evident moving further downstream.

The dependence of propulsive efficiency η on St for the different θ_0 cases at $Re = 750$ is illustrated in figure 10(*a*). The qualitative trends for all the θ_0 cases investigated are similar to the one seen earlier for $\theta_0 = 5°$, despite formation of a relatively strong leading edge vortex at higher θ_0. There are, however, some quantitative differences. In particular, a noticeable shift to higher St_{max} with increasing θ_0 is observed (at $Re = 750$, St_{max} increases from 0.48 to 0.66 as θ_0 is varied from 2° to 16°). Thus, for $Re = 750$, St_{max} does not saturate with θ_0. Our simulations indicate that this observation continues to hold even at a higher pitching amplitude of $\theta_0 = 24°$, in which case we find $St_{max} = 0.8$ with the corresponding maximum

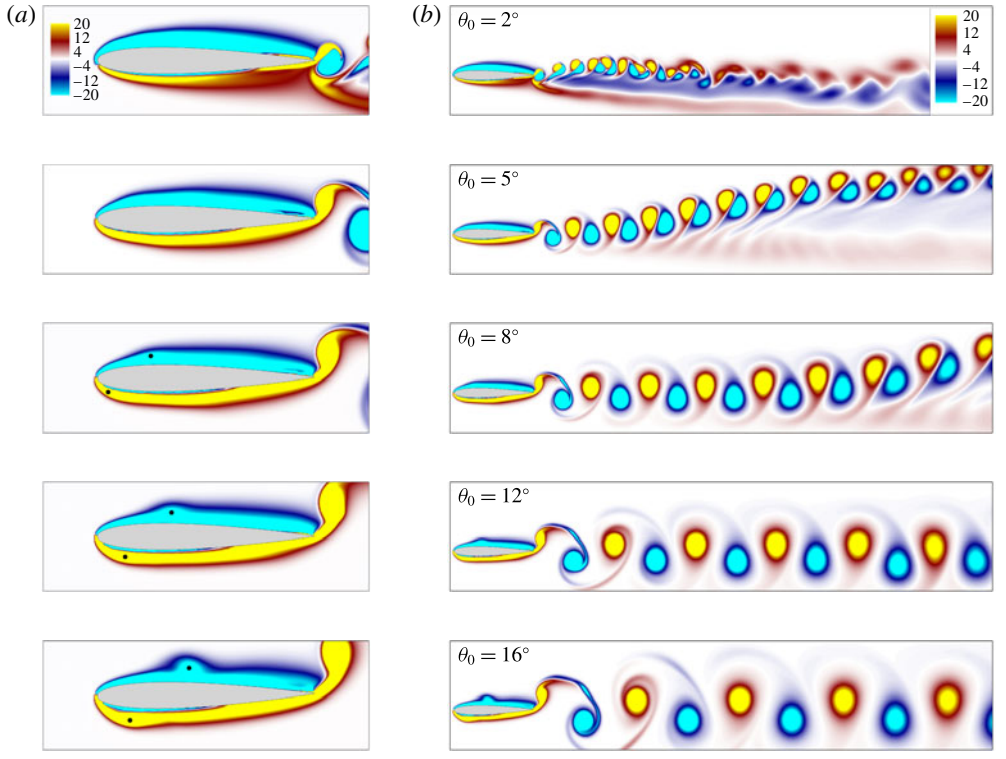

FIGURE 9. (Colour online) Effect of θ_0 on the vorticity field at $St = 0.4$ and $Re = 750$ for time instants at which the location of the pitching airfoil coincides with its mean position and when the trailing edge moves downwards. (*a*) A zoomed-in view around the airfoil. Filled circles (•) in (*a*) indicate the local maximum of the Q-criterion for leading edge vortex identification.

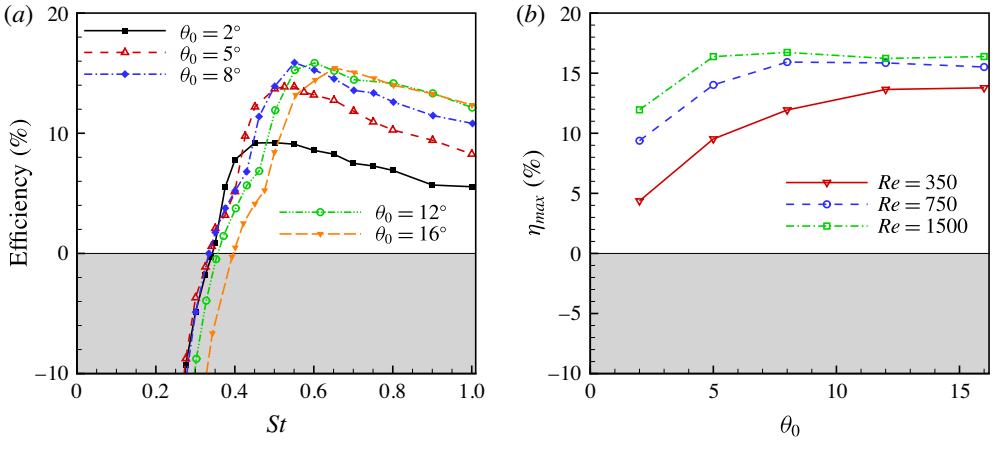

FIGURE 10. (Colour online) (*a*) Propulsive efficiency η as a function of St at $Re = 750$ for $\theta_0 = 2°$, 5°, 8°, 12° and 16°. (*b*) Maximum propulsive efficiency η_{max} as a function of θ_0 (in degrees) for $Re = 350$, 750 and 1500.

propulsive efficiency $\eta_{max} = 14\,\%$. Hence, at $Re = 750$, St_{max} exhibits significant dependence on θ_0. On the contrary, the peak efficiency η_{max} is found to be weakly dependent on θ_0, with relatively small changes in the maximum propulsive efficiency (η_{max}) between θ_0 of 5° and 16°. The dependency of η_{max} on Re and θ_0, as depicted in figure 10(*b*), shows that even the above mentioned small changes in η_{max} at a fixed Re of 750 (from figure 10*a*) are quite insignificant. At a fixed Re, η_{max} is found to increase with θ_0, and reach a nearly constant value beyond a certain θ_0, this value being approximately 8° at $Re = 750$ and 5° at $Re = 1500$. These results suggest that at large Re, the maximum propulsive efficiency η_{max} is reasonably independent of θ_0, and close to approximately 16 %, for all the cases considered in this work. This weak dependence of η_{max} on θ_0 is also consistent with the measurements of Mackowski & Williamson (2015) at moderate values of θ_0 considered here. This is however in contrast to the heaving foil case, where the results of Lewin & Haj-Hariri (2003) indicate that the propulsive efficiency is significantly affected by the nature of the interaction between the leading and trailing edge vortices.

6. Conclusions

In conclusion, a systematic evaluation of the energetic cost of thrust production from a NACA 0012 foil pitching about its quarter chord with an angular amplitude of 5° was performed numerically over a wide range of Reynolds ($10 \leqslant Re \leqslant 2000$) and Strouhal numbers with a high-resolution viscous vortex particle method. The numerical data for the time-averaged power coefficient exhibited a near-perfect collapse on a power-law scaling $\overline{C_P} \sim St^3$ almost independent of Re, as would be expected from a strong inertial dependency. In contrast, the time-averaged thrust coefficient $\overline{C_T}$ was found to significantly rise with Re in addition to the monotonic increase with St. The variation of $\overline{C_T}$ with St, and consequently the propulsive efficiency, $\eta = \overline{C_T}/\overline{C_P}$, showed a distinct steep increase that was linked to the observed shift in streamwise location at which the wake vortices undergo a deflection from the wake centreline. An increase in St beyond the value at which the asymmetry in the wake begins at the trailing edge of the foil led to only a marginal rise in η. Further increase in St lead to a peak followed by an eventual asymptotic decline ($\eta \sim St^{-1}$) that was consistent with the inertial scalings for the mean power and thrust coefficients at high St and Re. Most importantly, the peak propulsive efficiency (η_{max}), at a given Re, increased sharply with Re till $Re = 1000$, beyond which it showed a gradual saturation to an asymptotic value of approximately 16 %. This global peak propulsive efficiency of 16 % predicted from our simulations agrees reasonably well with previous higher Re experimental and numerical results on pitching foils. Additional simulation runs at angular pitching amplitudes of 2°, 8°, 12° and 16° confirmed this peak to be relatively insensitive to variations in θ_0 over the range $\theta_0 \leqslant 16°$.

A comprehensive characterization of the wake was performed over the range of Reynolds ($10 \leqslant Re \leqslant 2000$) and Strouhal numbers ($St \leqslant 1$). The resulting regime map clearly shows the strong effect of Re in addition to St for $Re < 1000$, with the effect of Re becoming gradually insignificant for $Re > 1000$. The map shows that the von Kármán to reverse von Kármán wake transition precedes the drag-to-thrust transition at all Re. Further, the Strouhal number at which the transition occurred showed a remarkable agreement with a power scaling, $St_{tr} \sim Re^{-0.37}$, derived from a balance of the thrust generated from pitching motion and drag force arising out of skin friction. The corresponding power coefficient too exhibited remarkable consistency

with a power law, $\overline{C_{P,tr}} \sim Re^{-1.12}$ that was shown to naturally follow from our scaling analysis. The map also showed that St_{max} exceeded the St for the onset of asymmetry, so that the peak propulsive efficiency was always achieved in the deflected wake regime. An analysis of the mean pressure and viscous contributions to the thrust coefficient established that the steep increase in the propulsive efficiency and the resulting maximum in the deflected wake regime are caused principally by a sharp rise in the time-averaged pressure contribution to the thrust from the leading edge of the airfoil.

Pitching foils are one of the many flapping foil based propulsion configurations which include, among others, heaving and combined pitching and heaving. In the case of heaving foils, lower Re results ($Re = 500$) of Lewin & Haj-Hariri (2003) and Martín-Alcántara, Fernandez-Feria & Sanmiguel-Rojas (2015) show that the peak propulsive efficiency is approximately 10 %. On the other hand, Heathcote & Gursul (2007) have shown that for a heaving foil, the propulsive efficiency and other global flow features at Re of 10 000, 20 000 and 30 000 are significantly higher (approximately 28 %) and nearly the same. This suggests that, as in the pitching case, there exists a threshold Re below which the performance drops considerably. Given these similarities, we expect the findings from our work to generalize to other flapping foil based propulsive systems with each configuration having a threshold Re below which the performance degrades considerably. This could be an important input for the design of small vehicles based on flapping propulsion. Our ongoing work is focused on exploration of such universal trends across general thrust generating flapping foil configurations.

Acknowledgements

The authors acknowledge support received from the NVIDIA Corporation (hardware donation program) and Supercomputing Education and Research Center-Indian Institute of Science (runtime on Cray XC40). The second author acknowledges support from the Department of Science and Technology (DSTO 1329).

Supplementary material

Supplementary material is available at http://dx.doi.org/10.1017/jfm.2016.399.

REFERENCES

ANDERSON, J. M., STREITLIEN, K., BARRETT, D. S. & TRIANTAFYLLOU, M. S. 1998 Oscillating foils of high propulsive efficiency. *J. Fluid Mech.* **360**, 41–72.

BIRCH, J. M., DICKSON, W. B. & DICKINSON, M. H. 2004 Force production and flow structure of the leading edge vortex on flapping wings at high and low Reynolds numbers. *J. Expl Biol.* **207**, 1063–1072.

BOHL, D. G. & KOOCHESFAHANI, M. M. 2009 MTV measurements of the vortical field in the wake of an airfoil oscillating at high reduced frequency. *J. Fluid Mech.* **620**, 63–88.

COTTET, G.-H. & KOUMOUTSAKOS, P. 2000 *Vortex Methods: Theory and Practice*. Cambridge University Press.

DEWEY, P. A., BOSCHITSCH, B. M., MOORED, K. W., STONE, H. A. & SMITS, A. J. 2013 Scaling laws for the thrust production of flexible pitching panels. *J. Fluid Mech.* **732**, 29–46.

EHRENSTEIN, U. & ELOY, C. 2013 Skin friction on a moving wall and its implications for swimming animals. *J. Fluid Mech.* **718**, 321–346.

EHRENSTEIN, U., MARQUILLIE, M. & ELOY, C. 2014 Skin friction on a flapping plate in uniform flow. *Proc. R. Soc. Lond.* B **372**, 20130345.

ELDREDGE, J. D. 2007 Numerical simulation of the fluid dynamics of 2D rigid body motion with the vortex particle method. *J. Comput. Phys.* **221** (2), 626–648.

ELDREDGE, J. D., TOOMEY, J. & MEDINA, A. 2010 On the roles of chord-wise flexibility in a flapping wing with hovering kinematics. *J. Fluid Mech.* **659**, 94–115.

GAZZOLA, M., ARGENTINA, M. & MAHADEVAN, L. 2014 Scaling macroscopic aquatic locomotion. *Nat. Phys.* **10**, 758–761.

GODOY-DIANA, R., AIDER, J.-L. & WESFREID, J. E. 2008 Transitions in the wake of a flapping foil. *Phys. Rev.* E **77** (1), 016308.

GODOY-DIANA, R., MARAIS, C., AIDER, J.-L. & WESFREID, J. E. 2009 A model for the symmetry breaking of the reverse Bénard–von Kármán vortex street produced by a flapping foil. *J. Fluid Mech.* **622**, 23–32.

GOUDE, A. & ENGBLOM, S. 2013 Adaptive fast multipole methods on the GPU. *J. Supercomput.* **63** (3), 897–918.

HARBIG, R. R., SHERIDAN, J. & THOMPSON, M. C. 2013 Reynolds number and aspect ratio effects on the leading-edge vortex for rotating insect wing planforms. *J. Fluid Mech.* **717**, 166–192.

HEATHCOTE, S. & GURSUL, I. 2007 Flexible flapping airfoil propulsion at low Reynolds numbers. *AIAA J.* **45**, 1066–1079.

HUNT, J. C. R., WRAY, A. A. & MOIN, P. 1988 Eddies, streams, and convergence zones in turbulent flows. In *Center for Turbulence Research Report CTR-S88*, pp. 193–208. NASA Ames/Stanford University Center for Turbulence Research.

KATZ, J. & WEIHS, D. 1978 Hydrodynamic propulsion by large amplitude oscillation of an airfoil with chordwise flexibility. *J. Fluid Mech.* **88**, 485–497.

KOOCHESFAHANI, M. M. 1989 Vortical patterns in the wake of an oscillating airfoil. *AIAA J.* **27** (9), 1200–1205.

KOUMOUTSAKOS, P. 2005 Multiscale flow simulations using particles. *Annu. Rev. Fluid Mech.* **37** (1), 457–487.

LEWIN, G. C. & HAJ-HARIRI, H. 2003 Modelling thrust generation of a two-dimensional heaving airfoil in a viscous flow. *J. Fluid Mech.* **492**, 339–362.

LIGHTHILL, M. J. 1971 Large-amplitude elongated-body theory of fish locomotion. *Proc. R. Soc. Lond.* B **179**, 125–138.

LIGHTHILL, M. J. 1975 *Mathematical Biofluiddynamics*. SIAM.

LU, K., XIE, Y. H. & ZHANG, D. 2013 Numerical study of large amplitude, nonsinusoidal motion and camber effects on pitching airfoil propulsion. *J. Fluids Struct.* **36**, 184–194.

MACKOWSKI, A. W. & WILLIAMSON, C. H. K. 2015 Direct measurement of thrust and efficiency of an airfoil undergoing pure pitching. *J. Fluid Mech.* **765**, 524–543.

MARTÍN-ALCÁNTARA, A., FERNANDEZ-FERIA, R. & SANMIGUEL-ROJAS, E. 2015 Vortex flow structures and interactions for the optimum thrust efficiency of a heaving airfoil at different mean angles of attack. *Phys. Fluids* **27** (7), 073602.

MCCROSKEY, W. J. 1982 Unsteady airfoils. *Annu. Rev. Fluid Mech.* **14**, 285–311.

OHMI, K., COUTANCEAU, M., DAUBE, O. & LOC, T. P. 1991 Further experiments on vortex formation around an oscillating and translating airfoil at large incidences. *J. Fluid Mech.* **225**, 607–630.

QUINN, D. B., LAUDER, G. V. & SMITS, A. J. 2015 Maximizing the efficiency of a flexible propulsor using experimental optimization. *J. Fluid Mech.* **767**, 430–448.

RAMAMURTI, R. & SANDBERG, W. 2001 Simulation of flow about flapping airfoils using finite element incompressible flow solver. *AIAA J.* **39** (2), 253–260.

SCHNIPPER, T., ANDERSEN, A. & BOHR, T. 2009 Vortex wakes of a flapping foil. *J. Fluid Mech.* **633**, 411–423.

SHYY, W., AONO, H., CHIMAKURTHI, S. K., TRIZILA, P., KANG, C.-K., CESNIK, C. E. S. & LIU, H. 2010 Recent progress in flapping wing aerodynamics and aeroelasticity. *Prog. Aerosp. Sci.* **46** (7), 284–327.

TAYLOR, G. K., NUDDS, R. L. & THOMAS, A. L. R. 2003 Flying and swimming animals cruise at a Strouhal number tuned for high power efficiency. *Nature* **425**, 707–711.

TRIANTAFYLLOU, M. S., TRIANTAFYLLOU, G. S. & YUE, D. K. P. 2000 Hydrodynamics of fishlike swimming. *Annu. Rev. Fluid Mech.* **32** (1), 33–53.

WANG, Z. 2000 Vortex shedding and frequency selection in flapping flight. *J. Fluid Mech.* **410**, 323–341.

WU, J.-Z., MA, H.-Y. & ZHOU, M.-D. 2007 *Vorticity and Vortex Dynamics*. Springer.

ZHU, X., HE, G. & ZHANG, X. 2014*a* How flexibility affects the wake symmetry properties of a self-propelled plunging foil. *J. Fluid Mech.* **751**, 164–183.

ZHU, X., HE, G. & ZHANG, X. 2014*b* Numerical study on hydrodynamic effect of flexibility in a self-propelled plunging foil. *Comput. Fluids* **97**, 1–20.